Normalizing the influence of flaw length on failure pressure of straight pipe with wall-thinning

Failure pressure of straight pipe with wall-thinning under internal pressure

Masayuki KAMAYA, Institute of Nuclear Safety System, Inc., (corresponding author)
Address: 64 Sata Mihama-cho, Fukui, JAPAN
Tel: +81 770 379114
Fax: +81 770 372009
E-mail: kamaya@inss.co.jp

Tomohisa SUZUKI, University of Fukui
Toshiyuki MESHII, University of Fukui

Abstract

The failure pressure of pipe with wall-thinning was investigated by using three-dimensional elastic-plastic finite element analyses (FEA). With careful modeling of the pipe and flaw geometry in addition to a proper stress-strain relation of the material, FEA could estimate the precise burst pressure obtained by the tests. FEA was conducted by assuming three kinds of materials: line pipe steel, carbon steel, and stainless steel. The failure pressure obtained using line pipe steel was the lowest under the same flaw size condition, when the failure pressure was normalized by the value of unflawed pipe defined using the flow stress. On the other hand, when the failure pressure was normalized by the results of FEA obtained for unflawed pipe under various flaw and pipe configurations, the failure pressures of carbon steel and line pipe steel were almost the same and lower than that of stainless steel. This suggests that the existing assessment criteria developed for line pipe steel are applicable to making a conservative assessment of carbon steel and stainless steel.

Key words: wall thinning, internal pressure, failure pressure, flaw length, material, finite element analysis, stainless steel

1. Introduction

Extensive studies have been conducted to assess the integrity of pipes containing wall-thinning under internal pressure. Through a number of experiments using full-scale specimens containing artificial wall-thinning as well as corroded pipes taken from actual pipelines, changes in the strength of wall-thinned pipe have been quantified [1], and empirical and semi-empirical assessment criteria developed for fitness-for-service [2][3]. On the other hand, numerical approaches have been taken based on the elastic shell theory [4][5] and finite element analysis (FEA). It was been shown that elastic-plastic FEA based

on shell modeling [6][7] and three-dimensional solid modeling [8][9] can be used to accurately estimate failure pressure.

The bursting of a pipe with wall-thinning accompanies a bulge due to inelastic deformation in the wall-thinned portion. Therefore, to accurately predict the burst pressure, it is important to consider the plastic deformation before bursting occurs. The deformation characteristic (stress-strain relation) is dependent on the material, and its influence on failure prediction has not been thoroughly discussed in previous studies. The assessment criteria were based on the elastic shell theory [4], and most of the previous studies were focused on such line pipe steel as X52[10], X60[1][10], X65[10][11], and X80[12] of the API standards. Conversely, in nuclear power plants, various materials are used in the piping systems and wall-thinning has occurred not only in carbon steel pipes but also in stainless steel pipes (e.g., at the Onagawa nuclear power plant, in May 2006). To ensure the integrity of plant components, it is important to clarify the influence of material properties on the failure strength of wall-thinned pipe as well as the effects of the shape of wall-thinning.

In this study, three-dimensional elastic-plastic FEA was conducted to examine the influence of the material and length of wall-thinning on the failure pressure. The wall-thinning was assumed to be of uniform depth circumferentially inside the straight pipe. The validity of FEA was confirmed by comparing its results with the experimental results obtained in a previous study conducted by the present authors [13]. Based on the FEA results, the influence of the material and length of the wall-thinned portion on failure pressure was discussed.

2. Experimental Procedure and Results [13]

An experiment was conducted using three specimens made from a carbon steel pipe for high-temperature use (STPT370 in JIS) with artificially introduced wall-thinning (hereafter called the 'flaw'). Figure 1 depicts the geometry of the specimens. Tables 1 and 2 list the chemical composition and mechanical properties of the material, respectively. The nominal outer diameter and thickness of the pipe were D_0 = 107.1 mm and t = 4 mm, respectively. In order to obtain uniform dimensions of diameter and thickness, the outer and inner pipe surfaces were machined before the flaw was introduced. The flaw was machined on the inside of the pipe to a depth of almost half the pipe thickness. The lengths of the flaw (in the longitudinal direction) of the three specimens were S_0 = 72.5 mm, 50 mm and 25 mm, respectively. The precise thickness of flawed portion was identified by measurements using an ultrasonic thickness gage. The depths of the flaws were approximately d = 2.1 mm, 2.2 mm, and 2.0 mm for the specimens with S_0 = 72.5 mm, 50 mm, and 25 mm, respectively.

In the tests, internal pressure was applied by injecting water into the pipe after evacuating air. The pressure at which the pipe burst was defined as the burst pressure (P_f). The results were P_f = 17.49 MPa, 18.17 MPa, and 23.90 MPa in the case of S_0 = 72.5 mm, 50 mm, and 25 mm, respectively.

3. Finite element analysis for experiment

3.1 Analysis Procedure

Three-dimensional elastic-plastic FEA was conducted using the general-purpose program ABAQUS, Version 6.5 [14]. Figure 2 schematically shows the geometry of a pipe with wall-thinning (flaw). The half-lengths of the flaw were S_0 = 72.5 mm, 50 mm, and 25 mm, respectively. The edge length (S_e) was 22.86 mm following the geometry of the specimen. The pipe length was set to $L = 5D_0$, which is sufficient to ignore the boundary effect at the end of the specimen. Since the failure pressure is sensitive to thickness at the wall-thinned portion, the thickness was determined by interpolating the measured thickness. In the experiment, thickness measurements at 34 points in the circumferential direction were made at every 10 mm in the longitudinal direction. Figure 3 shows the thicknesses at the longitudinal center ($z = 0$) and that at the end of the flawed portion. Table 3 summarizes the measurements. In the experiment, a longitudinal crack was initiated at the center of the flaw in the longitudinal direction, while the circumferential position is shown in Fig.3. The crack tended to be initiated in the relatively thin portion of the pipe, although no inhomogeneous bulging was not observed due to the uneven thickness during the experiments.

The pipe was modeled by using 8-node solid elements as shown in Fig.4. At the bottom of the flaw, the model was divided by four elements in the thickness direction and twenty elements in the longitudinal direction, with an element width of 5 degrees in the circumferential direction. There are 17280 elements and 24384 nodes included in the model shown in Fig. 4, which corresponds to the testing of S_0 = 50 mm. It was confirmed that well converged failure pressures were obtained with this mesh size. Axial tensile load was applied to the end of the pipe in order to simulate the end-capped condition.

Figure 5 shows the assumed the stress-strain relation (denoted as 'STPT') of the test material obtained using a tensile specimen for the circumferential direction. In the tests, large deformation (bulging) occurred before the pipe burst. Therefore, in order to simulate large inelastic deformation during the tests, the nonlinear geometry option (NLGEOM) with ABAQUS was invoked for the analysis procedure together with the modified Riks method, which allowed us to conduct analyses under the condition of static instability after plastic collapse. In the analyses, the internal pressure was increased until reaching a condition of instability. The maximum pressure during simulation was defined as the failure pressure, which was assumed to correspond to the burst pressure obtained in the experiment. The increase in pressure was controlled so as not to exceed 0.06MPa in the plastic region. The typical step size in pressure just before the failure was 0.001MPa.

3.2 Results of analysis

Table 4 lists the results of analysis together with the experimental results. The failure pressures obtained by the analyses agreed well with the experimental results. The error in

prediction by FEA was less than a maximum of 5%.

4. Influence of material and flaw geometry

4.1 Analysis Procedure

FEA was conducted for different flaw lengths and depths, and for material properties (stress-strain relations) under uniform flaw depth condition (Fig. 2). The pipe length and the edge of the flaw were set to $L = 5D_o$ and $S_e = 0.2S_o$, respectively. The equivalent flaw length (S) is defined by following equation:

$$S = \frac{A_o}{d}, \tag{1}$$

where A_o is the cross-sectional area of the flaw, and d is the depth of the flaw. Therefore, the equivalent flaw size was $1.1S_o$. Three stress-strain relations were assumed, as shown in Fig. 5. "X65" and "SS" correspond to line pipe steel [15] and stainless steel [16], respectively. The same procedure as used for the mesh division was adopted, although one-quarter of the full pipe was modeled due to geometrical symmetries. The displacement boundary conditions were applied to the planes of the symmetries and the axial tensile load was applied to the end of the pipe for the end-capped condition.

In order to evaluate the influence of the material and flaw length on the experimental results, FEA was initially conducted by assuming different flaw lengths and materials, but under the same pipe dimensions and constant flaw depth of $0.5t$. FEA was then conducted for various pipe configurations, which were possible combinations of diameter of 100A, 200A, 300A, 400A and 500A and the thickness of schedules 40 and 80 under different flaw depths of $d/t = 0.1$, 0.25, 0.5 and 0.75.

The analysis procedure in ABAQUS was the same as that used in the analyses for the experiment.

4.2 Results of analysis

Figure 6 shows the relationship between failure pressure P_f and the flaw size obtained by FEA for three materials under a constant flaw depth of $d = 0.5t$, together with the experimental results obtained using line pipe steel [11], low alloy steel [17], and carbon steel [13]. The data on carbon steel was obtained in our previous study and it should be noted that the depth of the artificial flaw in the tests was not exactly $0.5t$. The failure pressure is normalized by P_o, which is calculated by:

$$P_o = \frac{2}{\sqrt{3}}\sigma_f \frac{t}{R}, \tag{2}$$

where, σ_f is the flow stress defined as $\sigma_f = 0.5(\sigma_y + \sigma_b)$ using the yield strength (σ_y) and

ultimate strength (σ_b) of the test material. It was thus (288+447)/2, (450+568)/2 and (296+583)/2 in the case of STPT, X65 and SS, respectively. R denotes the nominal mean radius of the pipe in the unflawed section. Our previous study revealed that the pipe radius should normalize the influence of flaw length on the failure pressure [13]. Thus, in Fig. 6, R normalizes the flaw length.

The inclination of the curves for STPT and X65 are similar, although the intercept point at $S = 0$ is slightly different. On the other hand, SS exhibits a higher failure pressure than that of the other two materials. The failure pressures given in Ref.[11] were obtained by using X65 line pipe steel and agreed well with the FEA results using the X65 stress-strain curve. These results suggest that the failure pressure depends on the material properties. Stainless steel, in particular, exhibits unique changes with flaw length.

Figure 7 shows the failure pressures evaluated for various pipe and flaw configurations. The pressures were normalized by the value obtained for unflawed pipe. The normalized failure pressure is thus unity at $S = 0$. The failure pressure is dependent on the flaw depth and decreases with increases in flaw length, which is normalized by pipe mean radius R. This normalization yields a good correlation for all three materials, although normalization by the shell parameter $(Rt)^{0.5}$ or $(R(t-d))^{0.5}$ is used in the existing assessment criteria for wall-thinned pipe [18][19][20][21]. The results for STPT and X65 are almost identical, while SS exhibits better durability under the same flaw length.

5. Discussions

5.1 Failure pressure of unflawed pipe

In order to determine the failure assessment curve, it is important to set an adequate failure pressure for unflawed pipe, which in this study was assumed to be P_o. There are two principal issues in determining P_o. One is the end-capped effect, while the other is the definition of flow stress. The first issue should be considered when comparing the FEA results with experimental results, except in certain cases where the end-capped effect is intentionally excluded from the experiment [8][9] or where the Tresca criterion is predominant in determining the failure. When assessing integrity, however, multiplication by the factor $2/3^{0.5}$ should be dropped, since the axial load is not always expected especially in the intricate piping systems of nuclear power plants.

The second issue stems from the difference in deformation between the pipe and tensile specimen. The change in true stress against the strain of pipes during plastic deformation under internal pressure is not identical to that under uniaxial tension. That is to say, the true hoop stress ($S_h^{(t)}$) under internal pressure can be expressed as follows:

$$S_h^{(t)} = \frac{\sqrt{3}}{2} p \frac{R_i(1+e_h)}{t(1+e_h)^{-0.5}} = \frac{\sqrt{3}}{2} p \frac{R_i}{t}(1+e_h)^{1.5}, \quad (3)$$

where, e_h denotes the nominal hoop strain. Therefore, the true hoop stress is reduced by $(1+e_h)^{-0.5}$ from the value obtained in tensile test under the same strain. This suggests that the stress at plastic instability (pipe failure) is lower than the ultimate strength obtained by the tensile test. Various stresses have been used for the flow stress in Eq.(2) for the evaluation of wall-thinned pipes, such as σ_y + 10ksi [10][22][23], $\sigma_y/0.9$ [21], $1.1\sigma_y$ [19], and σ_b [24]. The results of the present study suggests that a flow stress of $\sigma_f = 0.5(\sigma_y + \sigma_b)$ yields a good approximation for estimating the failure pressure of unflawed pipe, and it is used in the fitness-for-service code of ASME [25] and JSME [26]. In addition, the validity of Eq.(2) has been demonstrated by burst tests using unflawed vessels with an end-cap [17].

5.2 Assessment criteria for failure pressure

As shown by the experiment and analyses, the failure pressure is dependent on flaw length. The failure pressure is near that of unflawed pipe (P_o) when the flaw length is small, and decreases as the flaw length becomes larger. When the flaw length is sufficiently large, the failure pressure should be equivalent to that of a pipe of thickness ($t - d$). There are thus two extremes in the failure pressure of pipe with wall-thinning. Leis and Stephens [27] proposed a concept in the following form:

$$\frac{P_f}{P_o} = 1 - \frac{d}{t} f(geometry). \qquad (4)$$

Here, $f(geometry)$ is a transition function connecting the two extremes, and related to the pipe and flaw geometry. The function can be obtained by interpolating the data shown in Fig. 7.

The existing failure assessment curves for wall-thinned pipe were mainly developed based on the data for line pipe steel or verified by tests conducted using line pipe steel [10][19][20][24]. The results shown in Figs. 6 and 7 suggest that these criteria can be used for making a conservative failure assessment of STPT370 carbon steel and stainless steel pipes.

6. Conclusions

The failure pressure of pipe containing wall-thinning was investigated by employing three-dimensional elastic-plastic FEA. Then, the influences of the material properties as well as the pipe geometry and flaw length were then investigated. The following conclusions were obtained:

a. The burst pressure can be estimated precisely by FEA with careful modeling of the pipe and flaw geometry in addition to a proper stress-strain relation of the material.
b. In the analyses of carbon steel, line pipe steel, and stainless steel, line pipe steel was

found to exhibit the lowest failure pressure under the same flaw size condition, when normalizing the failure pressure by the value of unflawed pipe as defined by using the flow stress.

c. For assessment criteria, the influence of the flaw length should be normalized by the pipe radius.
d. The failure pressure of unflawed pipe should be determined carefully, and the flow stress defined as the average of yield strength and ultimate strength gives good approximation of the failure pressure of unflawed pipe.
e. The existing assessment curves developed for line pipe steel can be used for making a conservative assessment of carbon steel and stainless steel pipes.

References

[1] Vieth PH, Kiefner JF. Database of corroded pipe tests. PRCI Catalog 1993; No.L51689.

[2] Turbak TA, Sims JR. Comparison of local thin area assessment methodologies. ASME PVP 1994; 288: 307-314.

[3] Stephens DR, Krishnaswamy P, Mohan R, Osage DA, Wilkowski GM .A review of analysis methods and acceptance criteria for local thinned areas in piping and piping components. ASME PVP 1997; 359: 55-65.

[4] Folias ES. An axial crack in a pressurized cylindrical shell. Int. J. Fracture Mech 1965; 1: 104-113.

[5] Kanninen MF. Pagalthivarthi KV, Popelar CH. A theoretical analysis for the residual strength of corroded gas and oil transmission pipelines. ASTM Special Technical Publication 1992; 1137: 183-198.

[6] Sims JR, Hantz BF, Kuehn KE. A basis for the fitness for service evaluation of thin areas in pressure vessels and storage tanks. ASME PVP 1992; 233: 51-58.

[7] Stephens DR, Leis BN. Material and geometry factors controlling the failure of corrosion defects in piping. ASME PVP 1997; 350: 3-11.

[8] Roy S. Grigory S. Smith M. Kanninen MF, Anderson M. Numerical simulations of full-scale corroded pipe tests with combined loading. Journal of Pressure Vessel Technology. 1997; 119: 457-466.

[9] Netto TA, Ferraz US, Estefen SF. The effect of corrosion defects on the burst pressure of pipelines. J. Constructional Steel Research 2005; 61: 1185-1204.

[10] Kiefner JF, Maxey WA, Eiber RJ, Duffy AR. Failure stress levels of flaws in pressurized cylinders. ASTM Special Technical Publication 1973; 536: 461-481.

[11] Kim YP, Baek JH, Kim WS, Kho YT. The evaluation of burst pressure for corroded pipeline by full scale burst test, Transactions of Korean Society of Mechanical Engineers 2002; 26: 203-210.

[12] Makino H, Takeuchi I, Tsukamoto M, Kawaguchi Y. Study on the propagating shear fracture in high strength line pipes by partial-gas burst test. ISIJ International 2001; 41: 788-794.

[13] Kamaya M, Suzuki T, Meshii T. Normalizing the influence of flaw length on failure pressure of straight pipe with wall-thinning. Nuclear Engineering and Design, doi:10.1016/j.nucengdes.2007.06.006.
[14] ABAQUS/Standard user's manual ver. 6.5. USA: ABAQUS Inc., 2005.
[15] Kim YJ, Shim DJ, Lim H, Kim YJ. Reference stress based approach to predict failure strength of pipes with local wall thinning under single loading, Journal of Pressure Vessel Technology 2004; 126: 194-201.
[16] Matsuoka S. Relationship between 0.2% proof stress and Vickers hardness of work-hardened low carbon austenitic stainless steel, 316SS. Transactions of the Japan Society of Mechanical Engineers 2004; A70: 1535-1541.
[17] Kobayashi H, Ogawa T, Yanagida S. Evaluation of corroded and artificially flawed vessels. Transactions of the Japan Society of Mechanical Engineers 2001; A67: 1688-1695.
[18] Cases of ASME boiler and pressure vessel code N-597-2 (Requirements for analytical evaluation of pipe wall thinning). USA: ASME, 2003.
[19] ANSI/ASME B31G (Manual for determining the remaining strength of corroded pipelines. USA: ANSI/ASME, 1984.
[20] Vieth PH, Kiefner JF. A modified criterion for evaluating the remaining strength of corroded pipe. PRCI Catalog 1989; No.L51688.
[21] API 579 (Fitness-for-service). USA: American Petroleum Institute, 2000.
[22] Kiefner JF, Vieth PH. A modified criterion for evaluating the remaining strength of corroded pipe, American Gas Association Catalog 1989; No.L51609.
[23] Chouchaoui BA, Pick RJ, Yost DB. Burst pressure predictions of line pipe containing single corrosion pits using the finite element method. OMAE 1992; V-A: 203-210.
[24] Leis BN, Shephens DR. An alternative approach to assess the integrity of corroded line pipe -part II: alternative criterion. 7th Int. Offshore and Polar Engineering Conference 1997; IV: 635-641.
[25] ASME boiler and pressure vessel code section XI. USA: ASME, 2004.
[26] Codes for nuclear power generation facilities: rules of fitness–for– service for nuclear power plants. Japan: JSME, 2004.
[27] Leis BN, Shephens DR. An alternative approach to assess the integrity of corroded line pipe -part I: current status. 7th Int. Offshore and Polar Engineering Conference 1997; IV: 624-634.

Captions

Table 1 Chemical composition of test material (wt %).
Table 2 Mechanical properties of test material.
Table 3 Summary of thickness measurement of wall-thinned portion.
Table 4 Comparison of failure pressure obtained by tests and finite element analyses.

Fig.1 Geometry of specimen for burst test.

Fig.2 Geometry of a pipe with wall-thinning for analyses.
Fig.3-1 Thickness of flawed portion (S_0 = 72.5 mm).
(a) z = 0
(b) z = 70 mm
(c) z = -70 mm
Fig.3-2 Thickness of flawed portion (S_0 = 50 mm).
(a) z = 0
(b) z = 50 mm
(c) z = -50 mm
Fig.3-3 Thickness of flawed portion (S_0 = 25 mm).
(a) z = 0
(b) z = 20 mm
(c) z = -20 mm
Fig.4 Finite element mesh for pipe with wall-thinning.
(a) Whole view
(b) Magnified cross sectional view of flawed portion
Fig.5 Stress-strain relation used in analyses.
Fig.6 Change in failure pressure due to material property and flaw length.
Fig.7 Relationship between the failure pressure and flaw length for various pipe geometries and materials.

Table 1 Chemical composition of test material (wt %).

C	Si	Mn	P	S	Fe
0.19	0.19	0.40	0.021	0.02	Bal.

Table 2 Mechanical properties of test material.

	Yield strength	Tensile strength	Elongation
Mill Sheet	288 MPa	447 MPa	0.4
Circumferential Direction	260 MPa	446 MPa	0.37

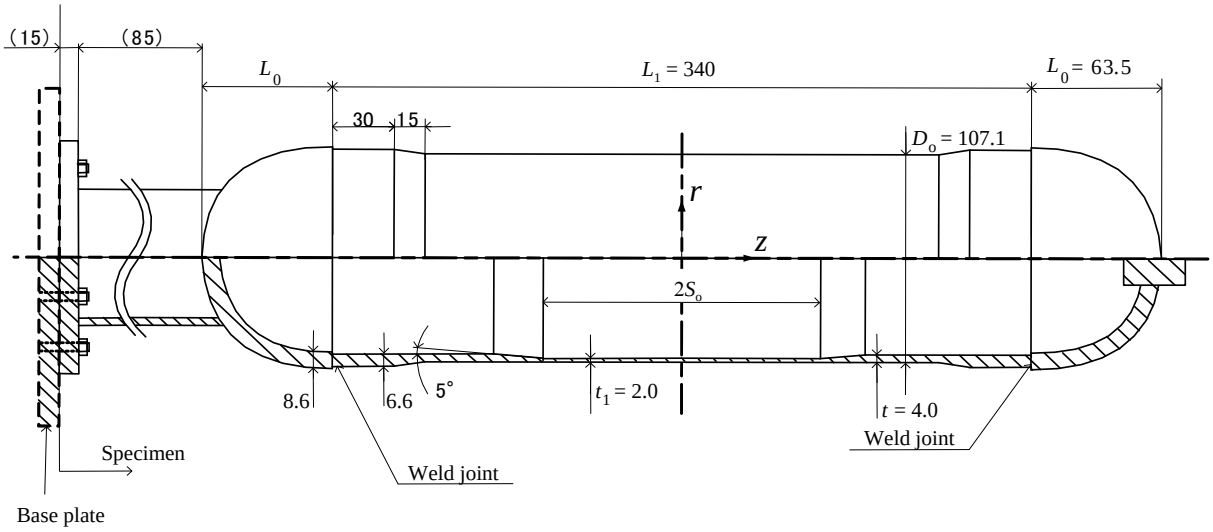

Fig.1 Geometry of specimen for burst test.

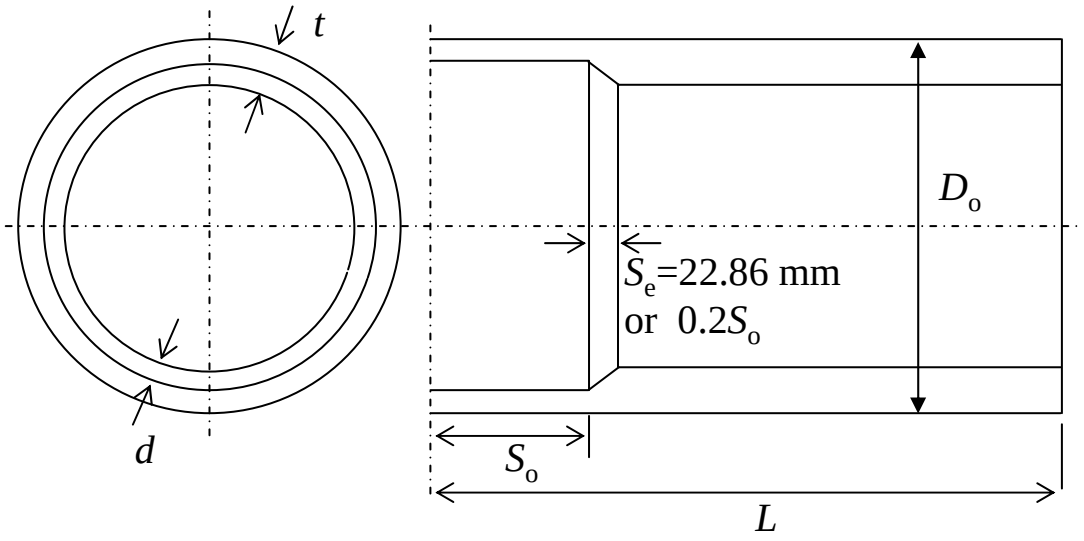

Fig.2 Geometry of a pipe with wall-thinning for analyses.

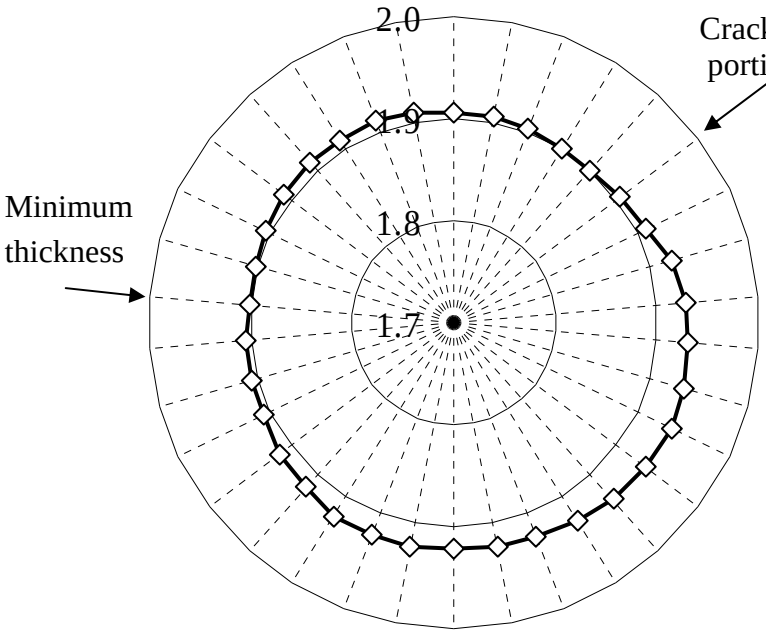

(a) z = 0

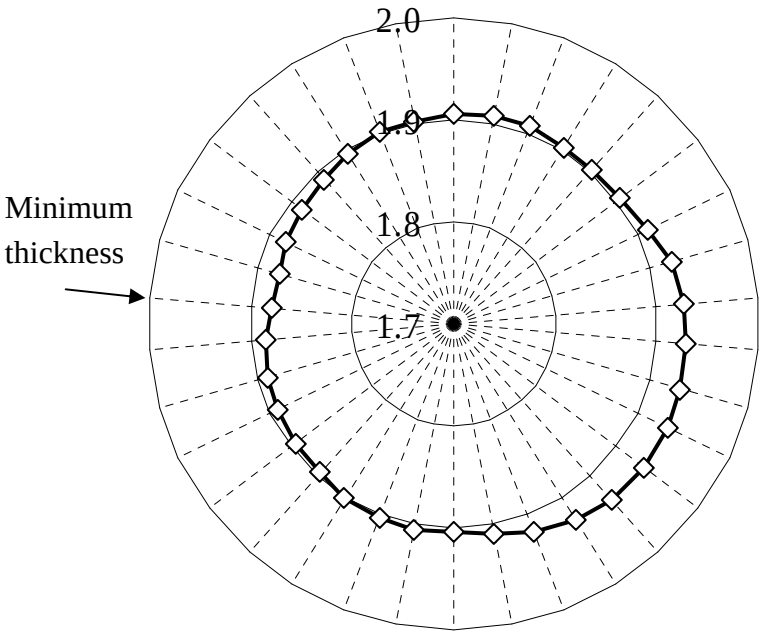

(b) z = 70 mm

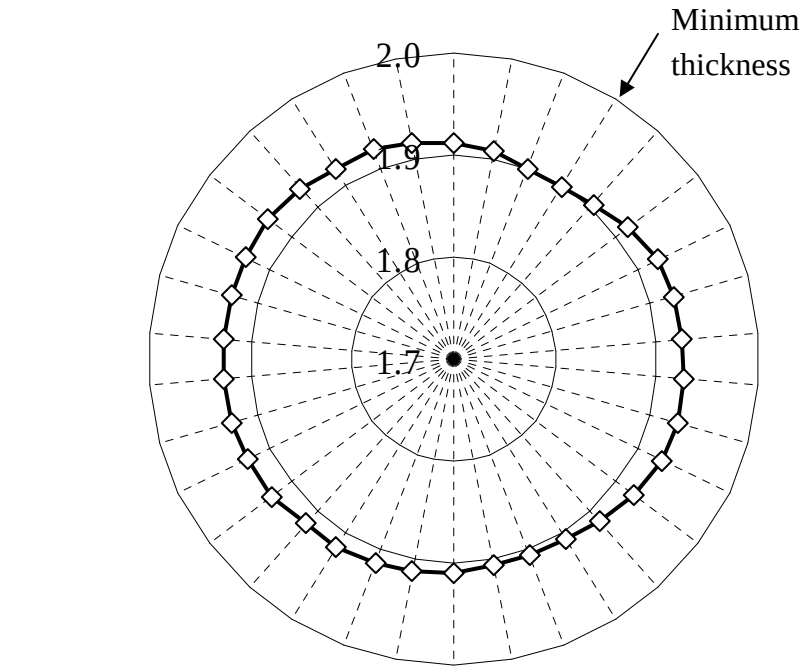

(c) z = -70 mm

Fig.3-1 Thickness of flawed portion (S_o = 72.5 mm).

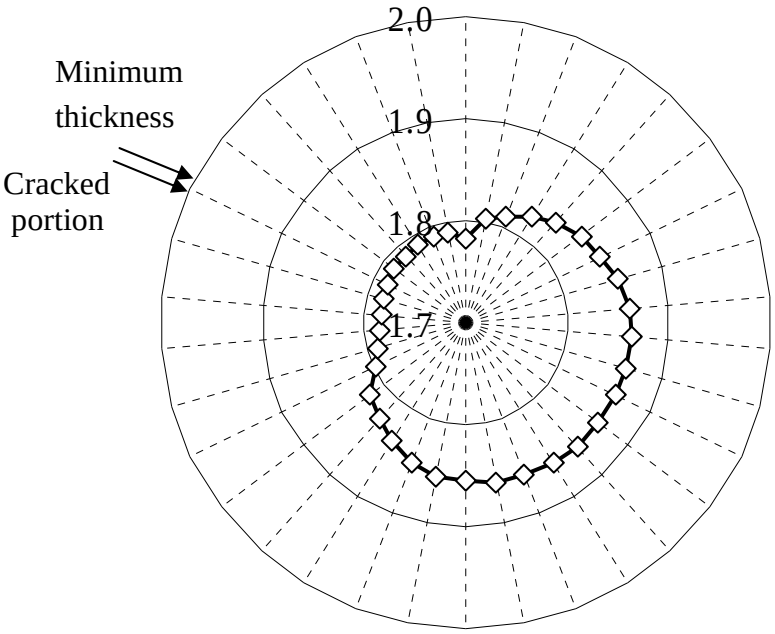

(a) z = 0

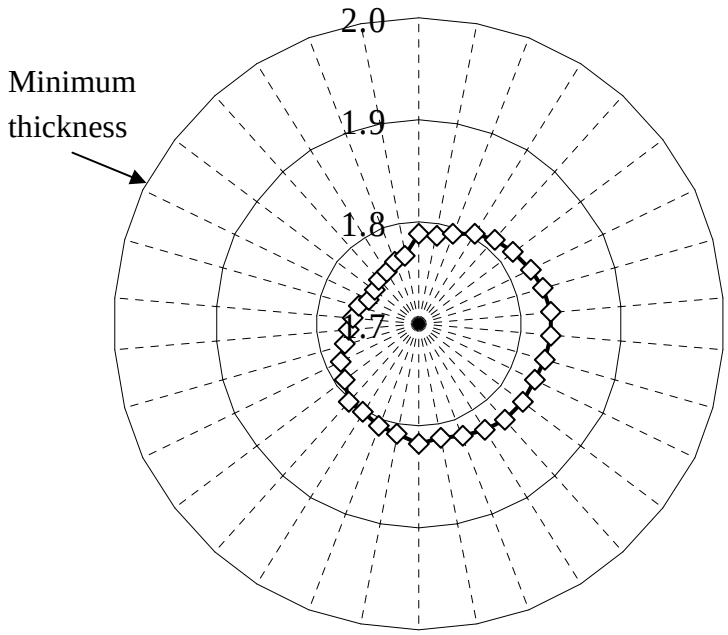

(b) z = 50 mm

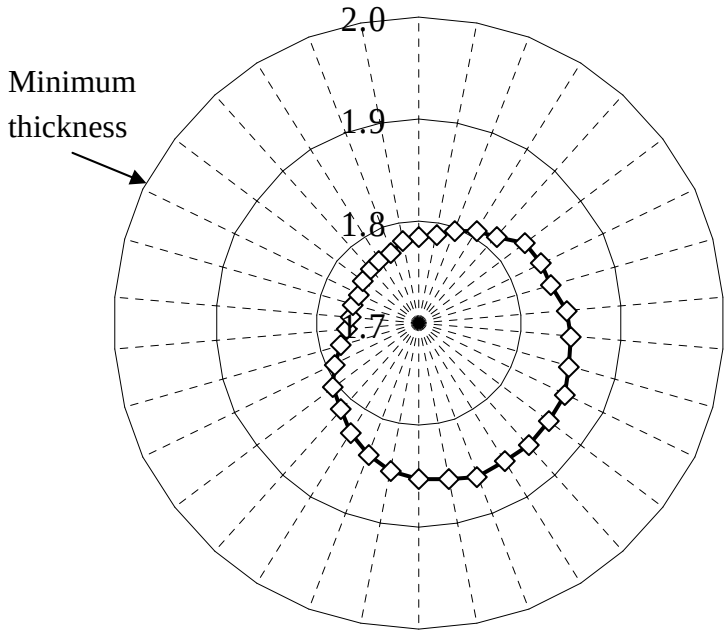

(c) z = -50 mm

Fig.3-2 Thickness of flawed portion (S_o = 50 mm).

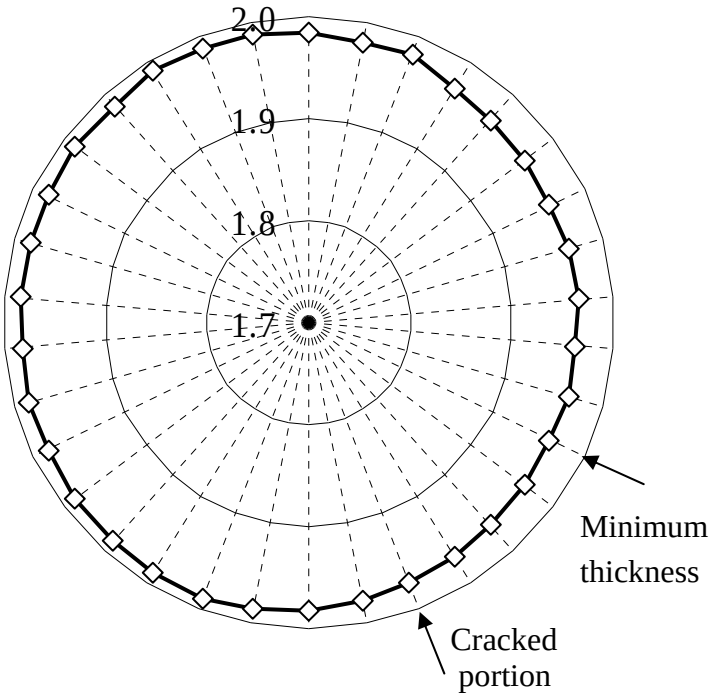

(a) z = 0

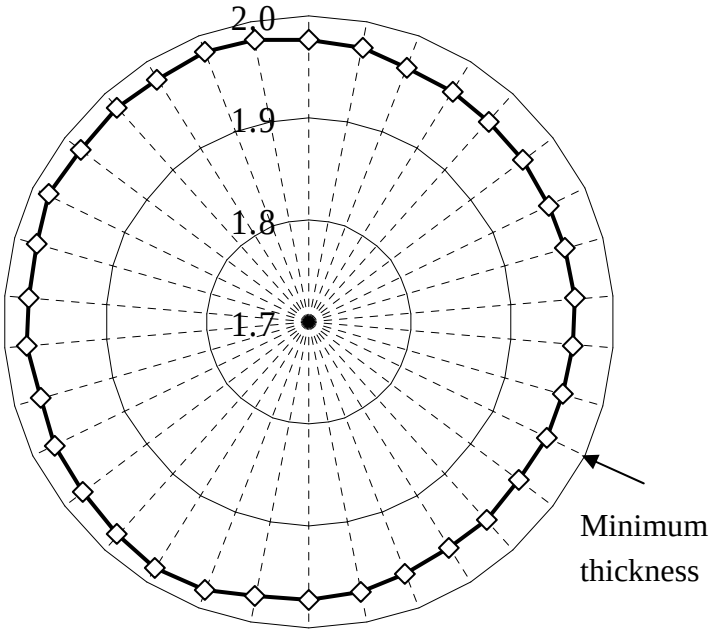

(b) z = 20 mm

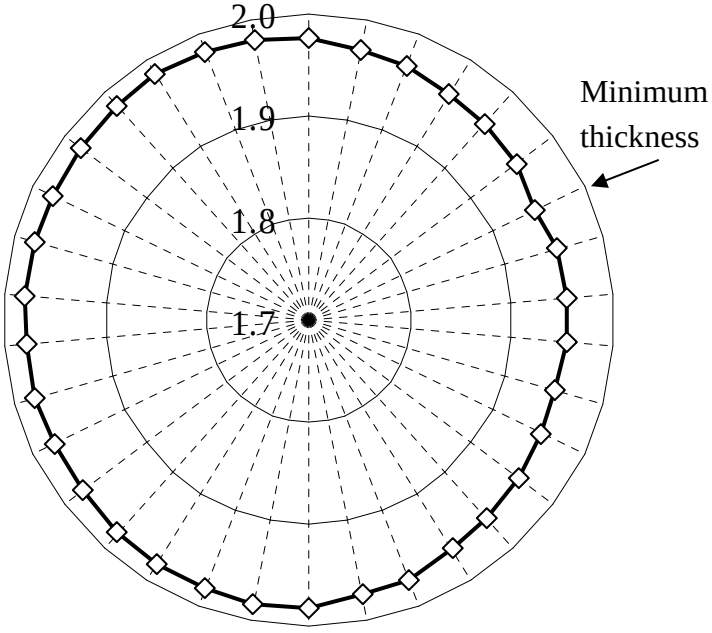

(c) z = -20 mm

Fig.3-3 Thickness of flawed portion (S_o = 25 mm).

Table 3 Summary of thickness measurement of wall-thinned portion.

Specimen (S_o)		Total	Center (z = 0)
72.5 mm	Number of data	360	34
	Average (mm)	1.91	1.92
	Minimum (mm)	1.87	1.90
	Maximum (mm)	1.95	1.94
50 mm	Number of data	264	34
	Average (mm)	1.81	1.82
	Minimum (mm)	1.76	1.78
	Maximum (mm)	1.87	1.86
25 mm	Number of data	170	34
	Average (mm)	1.97	1.98
	Minimum (mm)	1.95	1.96
	Maximum (mm)	1.99	1.99

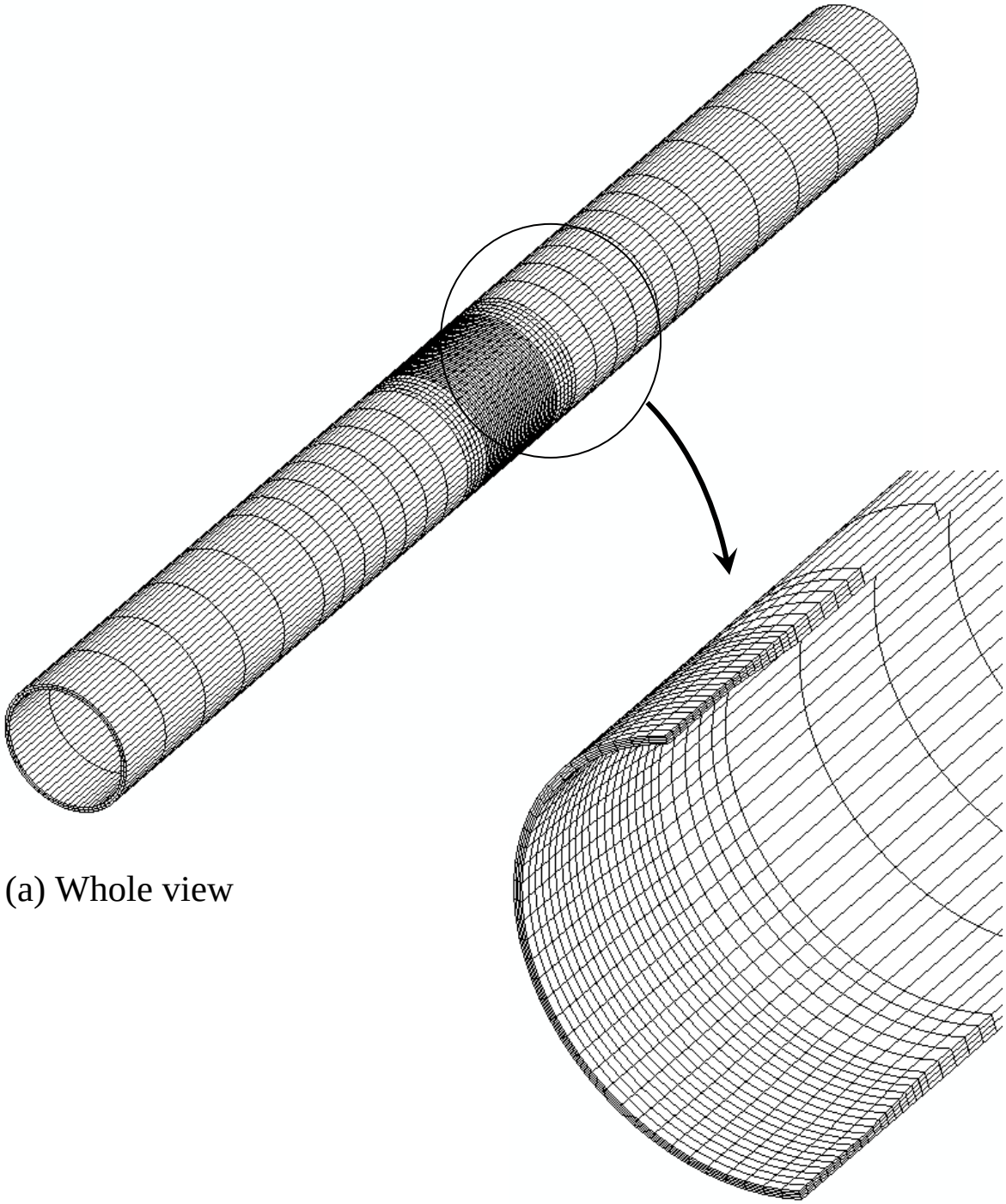

(a) Whole view

(b) Magnified cross sectional view of flawed portion

Fig.4 Finite element mesh for pipe with wall-thinning.

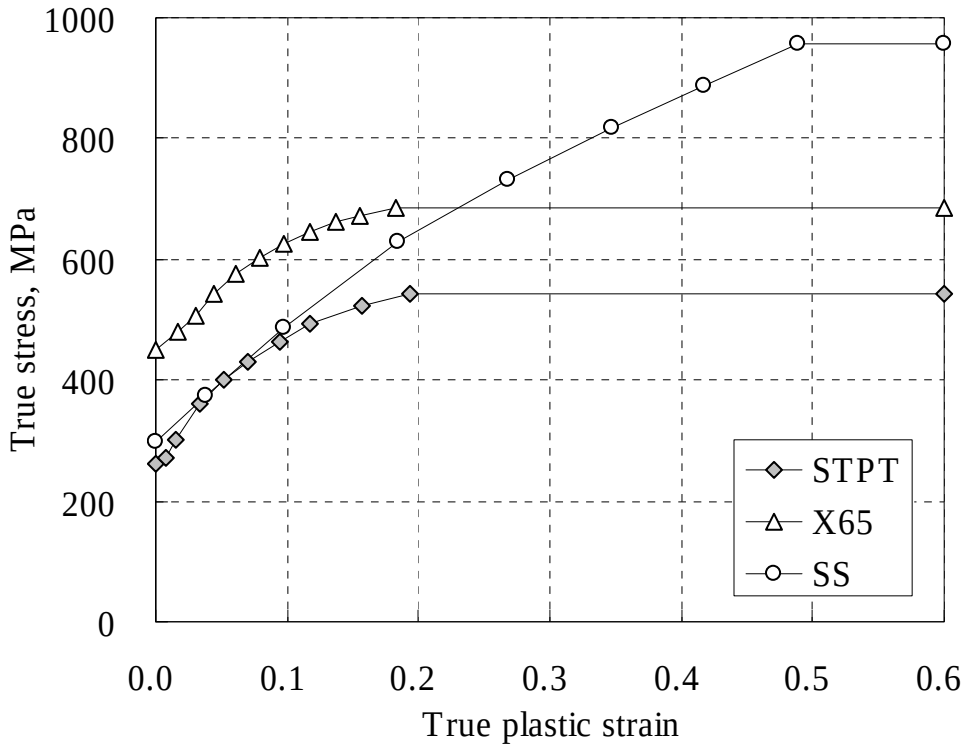

Fig.5 Stress-strain relation used in analyses.

Table 4 Comparison of failure pressure obtained by tests and finite element analyses.

Specimen (S_o)	Burst pressure (from tests) (MPa)	Failure pressure (form FEA) (MPa)	Error (%)
	A	B	(B-A)/A
72.5 mm	17.49	17.90	2.34
50 mm	18.17	18.03	-0.77
25 mm	23.90	22.90	-4.18

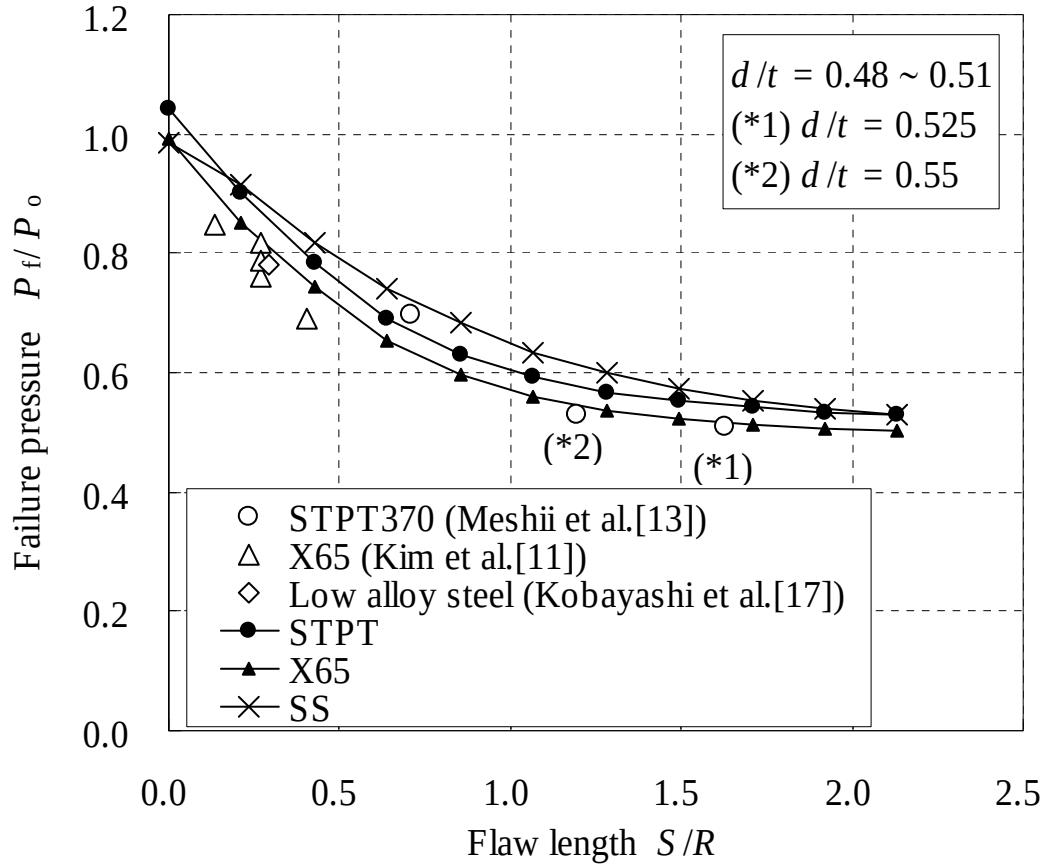

Fig.6 Change in failure pressure due to material property and flaw length.

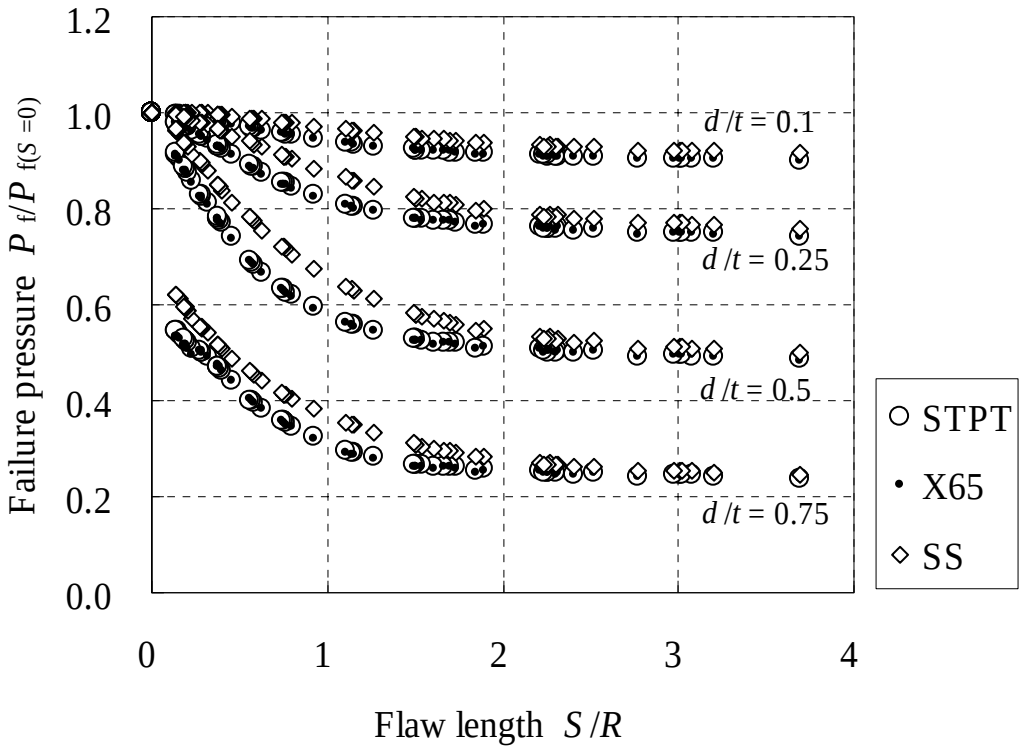

Fig.7 Relationship between the failure pressure and flaw length for various pipe geometries and materials.